Inherent Mach-Zehnder interference with "which-way" detection for single-particle scattering in one dimension

Lan Zhou (周兰),[1] Yue Chang (常越),[2] H. Dong (董辉),[2] Le-Man Kuang (匡乐满),[1] and C. P. Sun (孙昌璞)[2,*]

[1]*Department of Physics, Key Laboratory of Low-Dimensional Quantum Structures and Quantum Control of Ministry of Education, Hunan Normal University, Changsha 410081, China*

[2]*Institute of Theoretical Physics, Chinese Academy of Sciences, Beijing, 100190, China*

(Received 22 September 2011; published 4 January 2012)

We study the coherent transport of a single photon in a one-dimensional coupled-resonator array, nonlocally coupled to a two-level system. Since its inherent structure is a Mach-Zehnder interferometer, we explain the destructive interference phenomenon of the transmission spectra according to the effect of which-way detection. The quantum realization of the present model is a nanoelectromechanical resonator array with two nearest resonators coupled to a single spin via their attached magnetic tips. Its classical simulation is a waveguide of a coupled-defected cavity array with double couplings to a side-defected cavity.

DOI: 10.1103/PhysRevA.85.013806 PACS number(s): 42.50.Pq, 37.30.+i, 42.50.Ct

I. INTRODUCTION

In quantum mechanics, Bohr's complementarity principle for wave-particle duality could be displayed in various double-slit experiments (DSEs) [1]. It manifests that a detection about which way a particle takes in a DSE inevitably destroys quantum interferences, thus, the particle behavior (spatially localized) emerges while wavelike behavior (interference) disappears. Otherwise, if the detectors (apparatuses or environments) cannot distinguish the different possible paths well, the interference recovers [2–4]. Many experiments have tested this duality property through the which-way detection [5–8]. In this paper, we show the effect of which-way detection in a class of experimentally accessible systems with an inherent structure of the Mach-Zehnder interferometer where two virtual paths intrinsically are embedded.

We illustrate this observation with a single particle (photon or phonon) propagating in a one-dimensional coupled-resonator array (CRA) where a localized two-level system (TLS) simultaneously interacts with the confined electromagnetic (EM) field modes in two nearest resonators [illustrated in Fig. 1(a)]. The transported boson is scattered by the TLS when it enters one of these two nearest resonators, and then, the transmission and reflection spectra exhibit the interference pattern of the two scatterings. One may superpose these two local EM modes according to their couplings to the TLS [as illustrated in Fig. 1(b)]. Their antibonding superposition is decoupled with the TLS, while the only interaction between the bonding superposition and the TLS performs a which-way detection for the two virtual paths corresponding to the bonding and antibonding modes. In this inherent Mach-Zehnder interferometer with a which-way detector by the TLS, as the coupling strength increases gradually, the intrinsic interference in the scattering spectrum (the reflection and transmission spectra) disappears progressively. The reason is that the which-way detection only observes the particle motion in the antibonding branch. Therefore, the de-interference phenomenon for a single-particle scattering is understood in terms of the inherent Mach-Zehnder interferometer under the intrinsic which-way detection, which seems to be absent in the real configuration.

The paper is arranged as follows: In Sec. II, we introduce the model for demonstrating the Mach-Zehnder interference. In Sec. III, we study the single-photon propagating properties on this structure. The physical mechanism of the observed phenomena is explored in Sec. IV by taking advantage of the Mach-Zehnder interference. The possible physical realizations of the system are discussed in Sec. V. We conclude the paper in Sec. VI.

II. MODEL SETUP

The present system consists of a CRA and a side-coupled TLS. In contrast to the previous model [9–11], the TLS is coupled to two modes supported by two nearest resonators as illustrated in Fig. 1(a). The CRA is described by the model Hamiltonian under the nearest-neighbor approximation,

$$H_C = \sum_j \omega_c a_j^\dagger a_j - \sum_j \xi (a_{j+1}^\dagger a_j + \text{H.c.}), \tag{1}$$

with the annihilation-creation operator $a_j/a_j^\dagger$ of a confined boson (photon in a single-mode cavity or cooled phonon in a nanomechanical resonator) in the jth resonant cavity mode. This is a typical tight-binding boson model. For simplicity, we assume that all cavities have the same eigenfrequency ω_c and the intercavity coupling has the same strength ξ. In this array, waves propagate freely and are characterized by the dispersion relation,

$$\omega_k = \omega_c - 2\xi \cos k, \tag{2}$$

which forms a frequency band in a continuum spectrum.

The TLS with ground state $|g\rangle$, excited state $|e\rangle$, and energy-level spacing Ω, is coupled to two nearest cavities of the one-dimensional (1D) CRA with corresponding strengths g_0 and g_1. Under the rotating-wave approximation, the dynamics of the TLS interacting with the electromagnetic field is described by the Jaynes-Cummings Hamiltonian,

$$H_I = \Omega \sigma_{ee} + \sigma_-(g_0 a_0^\dagger + g_1 a_1^\dagger) + \text{H.c.}, \tag{3}$$

*suncp@itp.ac.cn; http://power.itp.ac.cn/~suncp

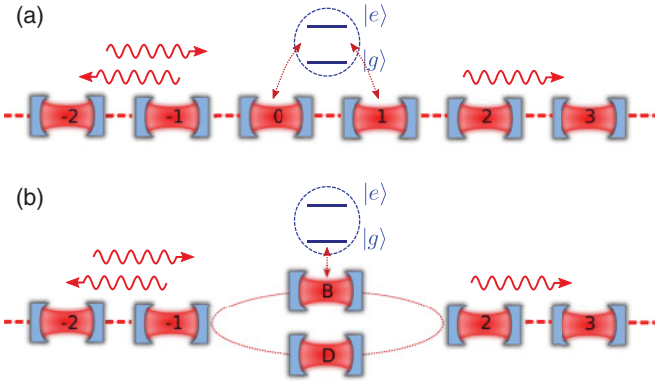

FIG. 1. (Color online) Schematic of the studied system and the physical mechanism. (a) The single boson (photon or phonon) scattered by a nonlocal TLS simultaneously coupled to two nearest resonators in a one-dimensional CRA and (b) the equivalent Mach-Zehnder interferometer with which-way measurement where the bonding and antibonding superpositions of the two local cavity modes form two paths for interference, one of which is probed by the TLS while the other is decoupled with it.

where the first term describes the free energy of the TLS with $\sigma_{ee} = |e\rangle\langle e|$. The operator $\sigma_- = |g\rangle\langle e|$ and its adjoint σ_+ are the corresponding lowing and rising operators. We remark that the present model can be implemented physically with a nanoelectromechanical resonator array or a defect resonator array on a photonic crystal. The detailed description will be presented in Sec. V.

III. SINGLE-PHOTON SCATTERING

It is clear that the number of excitations is conserved in this hybrid system. In the one-excitation subspace, two mutually exclusive possibilities are considered: The particle either is propagating inside the cavity or is absorbed by the TLS. It indicates that the eigenstate has the form

$$|E_k\rangle = \sum_j [u_{kj} a_j^\dagger |0g\rangle + u_{ke}|0e\rangle]. \tag{4}$$

From the Schrödinger equation $(H_C + H_I)|E_k\rangle = E_k|E_k\rangle$, we derive a series of coupled stationary equations for the excited-state amplitude u_{ke} and the amplitudes u_{kj} of single-photon states [9,10] in the jth cavity. Here, the part concerning the excited state,

$$(E_k - \Omega)u_{ke} = (g_0 u_{k0} + g_1 u_{k1})$$

leads to a dispersive coupling strength between the zeroth and the first resonators and a nonlocal effective potential,

$$V(j) = G(E_k)(|g_0|^2\delta_{j0} + |g_1|^2\delta_{j1}), \tag{5}$$

which is proportional to the Green's function $G(E_k) = (E_k - \Omega)^{-1}$. The single-excitation transport is described by the discrete-scattering equation,

$$(\omega_c - E_k)u_{kj} = \xi(u_{kj-1} + u_{kj+1}) + G(E_k)(g_j\delta_{j0} + g_j\delta_{j1})(g_0 u_{k0} + g_1 u_{k1}). \tag{6}$$

The first term on the right of Eq. (6) characterizes the hopping between different sites as the kinetic term. And the double-δ potentials in the send term are induced from the couplings between the TLS and the CRA. However, such δ potentials are nonlocal compared with the one-site coupling in Refs. [9–11]. Therefore, the coherent scattering by the two sites will bring different physical effects.

The process that an incident wave impinges upon the structure, where transmitted and reflected waves emerge, is formulated by assuming

$$u_k(j) = \exp(ikj) + r_k \exp(-ikj) \tag{7}$$

for $j \leqslant -1$ and

$$u_k(j) = t_k \exp(ikj) \tag{8}$$

for $j \geqslant 2$ with reflection and transmission amplitudes r_k and t_k. Concerning Eq. (6) with the zeroth and first resonators, with the above assumptions, we immediately obtain the transmission,

$$t_k = \frac{2i\ \sin k[(E_k - \Omega)\xi - g_0 g_1]}{2i\ \sin k(E_k - \Omega)\xi - 2g_0 g_1 e^{ik} - \left(g_1^2 + g_0^2\right)}, \tag{9}$$

and reflection amplitudes,

$$r_k = \frac{2i\ \sin k g_1^2 e^{ik} + 2g_0 g_1 e^{ik} + \left(g_1^2 + g_0^2\right)}{2i\ \sin k(E_k - \Omega)\xi - 2g_0 g_1 e^{ik} - \left(g_1^2 + g_0^2\right)}. \tag{10}$$

The eigenenergy $E_k = \omega_k$ is obtained by applying Eq. (6) to the resonators far away from the resonators at $j = -1$ to 2. It is checked that the reflection coefficient $R = |r_k|^2$ and transmission coefficient $T = |t_k|^2$ satisfy the identity $|r_k|^2 + |t_k|^2 = 1$.

In Eqs. (9) and (10), it is clear that the transmission generally vanishes at the band edges with $k = 0, \pi$. However, constructive interference is found at $k = \pi$ when $g_0 = g_1 = g$ (red solid line in Fig. 2). Compared to the case of one-site coupling (solid dotted line in Fig. 2), the transmission does not vanish at $E_k = \Omega$ with the nonvanishing amplitude,

$$t_{k_\Omega} = \frac{2ig_0 g_1\ \sin k_\Omega}{2g_0 g_1 \exp(ik_\Omega) + \left(g_1^2 + g_0^2\right)}, \tag{11}$$

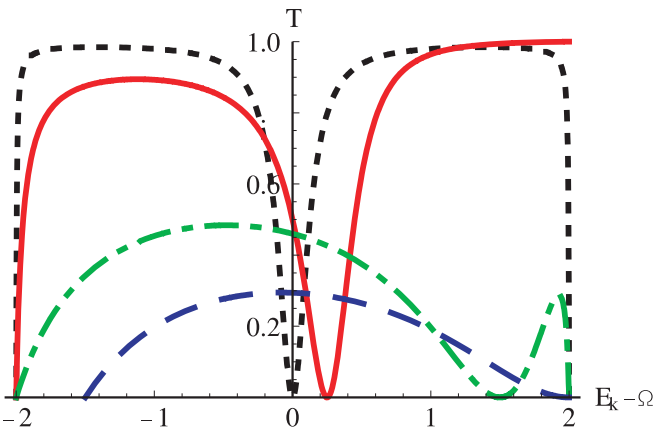

FIG. 2. (Color online) Transmission coefficient T with transition energy $\Omega = \omega_c = 2$ as a function of the photon incident energy E_k. The coupling strengths $g_0 = 0.5$ and $g_1 = 0$ for the black dotted line, $g_0 = g_1 = 0.5$ for the red solid line, $g_0 = 1$ and $g_1 = 1.5$ for the green dot-dashed line, and $g_0 = 1$ and $g_1 = 2.5$ for the blue dashed line. All parameters are in units of ξ.

due to the nonlocal coupling between the TLS and the CRA. Obviously, the position of transmission zero is shifted to $\Omega + g_0 g_1/\xi$. When the coupling gets stronger, the transmission dip gradually moves outside the spectrum band, thus, no transmission zero appears as shown in Fig. 2. The coupling between the TLS and the CRA induces effective double-δ potentials in the way of photon propagation. The strength tends to infinite potentials at $E_k = \Omega$, which indicates the total reflection. However, the straightforward physics picture fails to explain the nonvanishing transmission at $E_k = \Omega$ in the case of nonlocal coupling.

IV. DE-INTERFERENCE AND WHICH-WAY EXPLANATION

To give an intuitionistic explanation about the nonvanishing point of transmission, we now introduce the bonding and antibonding modes,

$$B = a_0 \cos\theta + a_1 \sin\theta,$$
$$D = -a_0 \sin\theta + a_1 \cos\theta,$$

where $\tan\theta = g_1/g_0$. When $g_0 = g_1 = g$, modes B and D present two virtual paths without direct coupling between each other, then the CRA virtually becomes an equivalent Mach-Zehnder interferometer [see Fig. 1(b)] where arm B experiences a which-way measurement by the TLS. Those cavities on the left of the cavity at $j = -1$ or on the right of the cavity at $j = 2$ are regarded as the left and right leads, which are connected to each other via two arms. The lower arm corresponds to the antibonding model D of eigenfrequency $\omega_D = \omega_c + \xi \sin 2\theta$, while the upper arm corresponds to the bonding mode B of eigenfrequency $\omega_B = \omega_c - \xi \sin 2\theta$ coupled to the TLS with coupling strength $\sqrt{2}g$. The effective hopping strengths between the bonding mode B and the nearby cavities are $\xi \cos\theta$ and $\xi \sin\theta$. It is emphasized that antibonding mode D indeed is decoupled with the TLS.

In the above equivalent configuration, the propagating state is a superposition of four mutually exclusive possibilities: (i) the particle propagating inside left and right leads, represented by state $a_j^\dagger|0g\rangle$ with possibility amplitude u_{kj}, (ii) absorbed by the TLS, by $u_{ke}|0e\rangle$, (iii) propagating from the left to right lead via the upper arm by $B^\dagger|0g\rangle$ with amplitude u_{kB}, or (iv) via the lower arm by $D^\dagger|0g\rangle$ with amplitude u_{kD}. The superposition of these four possibilities forms a stationary state $|E_k\rangle$ with the band energy E_k. Here, three scattering channels are implied, i.e., a single particle travels through the excited TLS or via the bonding and antibonding branches, respectively, with the TLS unexcited. In the reduced dimensionality, particles follow two different paths defined by two virtual modes. We refer to these two paths as paths B and D corresponding to the B slit and the D slit. A dispersion δ potential is localized in path B since the particle passing the B slit interacts with the TLS. The total transmission amplitude is the sum of the amplitudes in the two branches, and the interference pattern is determined by the phase difference between the two paths. Therefore, the suppression of quantum interference depends on the dwell time of the single particle absorbed by the TLS.

An incoming wave with energy E_k, incident from the left lead, is split into two branches at the first junction and joins again into the outgoing wave at the second junction. The propagation of the single particle around the ring [consisting of sites -1, D, B, and 2 shown in Fig. 1(b)] is described as follows: the discrete-scattering equation in path B,

$$(E_k - \omega_B)u_{kB} = \sqrt{2}g u_{ke} - \frac{\xi}{\sqrt{2}}(u_{k2} + u_{k-1}), \tag{12}$$

which is coupled to the local atomic excitation characterized by

$$(E_k - \Omega)u_{ke} = \sqrt{2}g u_{kB}.$$

In path D, the particle propagates freely with the motion equation $(E_k - \omega_D)u_{kD} = \xi(u_{k2} - u_{k-1})/\sqrt{2}$. However, on the nodes with $j = -1,2$, the amplitudes for the single particle are coupled to those two splitting nodes B and D, respectively, with the following forms:

$$(E_k - \omega_c)u_{k-1} = -\xi u_{k-2} - \frac{\xi}{\sqrt{2}}(u_{kB} + u_{kD}), \tag{13}$$

$$(E_k - \omega_c)u_{k2} = \frac{\xi}{\sqrt{2}}(u_{kD} - u_{kB}) - \xi u_{k3}. \tag{14}$$

Then, it follows from the above discrete-scattering equation that the transmission amplitude $t_k = t_k^D + t_k^B$ is given by the partial-wave transmission amplitude $t_k^D = i \sin(k/2)\exp(-ik/2)$ and

$$t_k^B = \frac{e^{-ik/2}\xi(E_k - \Omega)\cos(k/2)}{\xi(E_k - \Omega) - g^2 + ig^2\tan^{-1}(k/2)}, \tag{15}$$

in paths D (B), respectively, in the absence of paths B (D).

When the incident single particle is resonant to the TLS, the emitted wave from the TLS and the propagating modes in the 1D continuum lead to the complete suppression of the wave transmission in path B, then photons take path D. Therefore, the TLS prevents single-particle interference of paths B and D. In this sense, the TLS serves as a which-path detector. It is the potential exerted by the TLS that makes waves accumulate a phase on path B, then the wave interference of paths B and D displays a transmission zero in t_k. However, the coupling strength characterizes the time that the single-particle dwells in the TLS. Consequently, the interference pattern is expected to diminish as the coupling strength increases. Figure 3 shows the contour plots of transmission coefficient $|t_k|^2$ as a function of the incident energy E_k and coupling strength g. Here, we can see that, as coupling strength g increases, the complete suppression of the wave transmission begins at $E_k = \Omega$, gradually shifts to the band edge, and then disappears. One also may find that the perfect transmission at $k = \pi$ is independent of the potential exerted by the TLS. When $k = \pi$, the probability amplitudes $u_{kj} = (-1)^j$ for $j \neq 0,1$ lead to destructive interference at the B slit since $u_{kB} = 0$ and constructive interference at the D slit. In this case, the TLS effectively is decoupled from the CRA.

V. PHYSICAL IMPLEMENTATIONS

The above nonlocal coupling obviously distinguishes the present investigation from the previous extensive ones [9,10,12–14] where the TLS only is coupled to the EM field in a single cavity. Experimentally, the previous setups are feasibly implemented with the confined photons or the single-mode phonon in some confined nanostructures [15], e.g., the

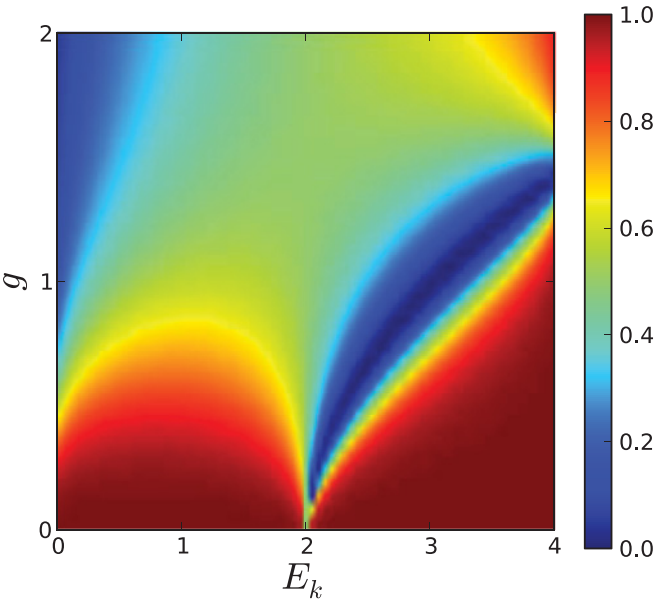

FIG. 3. (Color online) Transmission coefficient $|t_k|^2$. Its contour plot with respect to E_k and coupling strength g. All parameters are in units of ξ.

circuit QED system, a semiconductor quantum-dot coupling with nanoscale surface plasmons or the defect cavities of a photonic crystal, and the nano-electromechanical-resonator arrays where every resonator is coupled to a localized spin [16]. To implement the present nonlocal coupling seems difficult in the photonic CRA, but it could be feasible for the nano-electromechanical-resonator array coupled to a local spin, where two of the resonators are attached by magnetic tips producing magnetic fields in the x direction (see Fig. 4). With the charged resonators oscillating in the z direction and under the rotating-wave approximation, the inter-resonator coupling is realized via Coulomb forces [16], while two of them simultaneously interact with a single spin through the magnetic-field gradients [17]. In nano-electromechanical-resonator experiments, parameters ω_c, ξ, and Ω easily can reach a 10^6-Hz frequency scale, and the cavity-TLS coupling strength is on the order of 100 kHz. The second implementation of the nonlocal coupling could be in a two-dimensional (2D) photonic crystal [18], which is made up of a square lattice of high-index dielectric rods as illustrated in Fig. 4. Here, two nearest cavities in a waveguide of coupled-defected cavity arrays is coupled to a side-defected cavity. In the single-excitation subspace, the side cavity with two states (vacuum and single photon) simulates the TLS in our general setup.

We note that, in reality, there are no ideal resonators, leads, for example, different eigenfrequencies and coupling constants in the CRA. To study all the limiting factors due to material and device imperfections is not possible analytically since it would be necessary to use a microscopic model. So here, we only consider that the eigenfrequencies in the zeroth and first resonators are different, which are denoted as $\omega_c + \xi\bar{\omega}_0$ and $\omega_c + \xi\bar{\omega}_1$, and the coupling strength between zeroth and first cavities is different from the others, which is denoted by $\xi\eta$. Then, the Hamiltonian for the system reads

$$H = \sum_j [\omega_{cj} a_j^\dagger a_j - \xi_j (a_{j+1}^\dagger a_j + \text{H.c.})] + H_I,$$

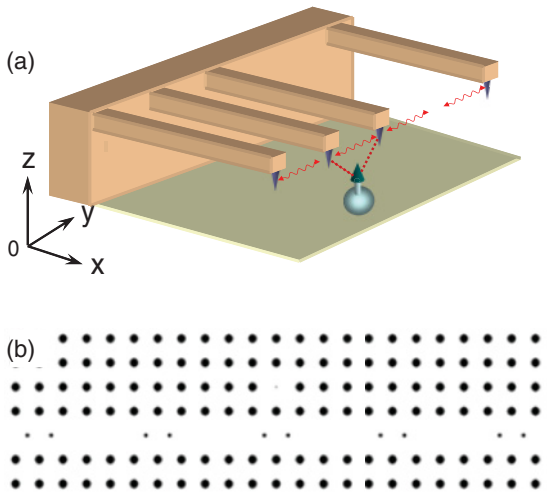

FIG. 4. (Color online) Two physical implementations: (a) nano-electromechanical-resonator arrays where two nearest resonators with ferromagnetic particles in the tips are coupled to a localized spin. The origin of the coordinate frame is at the spin. Here, all the resonators are charged so that they interact with neighboring ones via Coulomb forces (b). In the 2D photonic crystal, a side-defected cavity with double couplings to a waveguide of coupled-defected cavity arrays. In the single-excitation subspace, the side cavity with two states behaves as a TLS.

where the eigenfrequency of each resonator and the coupling strength between the resonators are defined as

$$\omega_{cj} = \omega_c + \xi\bar{\omega}_0\delta_{j0} + \xi\bar{\omega}_1\delta_{j1},$$
$$\xi_j = \xi + \xi(\eta - 1)(\delta_{j0} + \delta_{j1}).$$

The transmission spectrum has the following form

$$t_k = \frac{e^{-ik} 2i \sin k[\eta\xi(E_k - \Omega) - g_1 g_0^*]}{\eta_k \xi(E_k - \Omega) - (g_1 g_0^* + g_0 g_1^*)\eta - \bar{g}_k},$$

where we have defined

$$\eta_k = \eta^2 - (e^{-ik} + \bar{\omega}_0)(e^{-ik} + \bar{\omega}_1)$$
$$\bar{g}_k = |g_0|^2(e^{-ik} + \bar{\omega}_1) + |g_1|^2(e^{-ik} + \bar{\omega}_0).$$

It can be seen that the position of the total reflections shift from Ω to $\Omega + g_1 g_0^*/(\eta\xi)$, which is related to coupling strength $\eta\xi$ between the zeroth and the first cavities but is independent of the unequal eigenfrequencies of resonators in the CRA. This observation can be found in the scattering process of a photon on a CRA with one different eigenfrequency of resonators [19]. When only one resonator of the CRA has a different eigenfrequency, there is no total reflection unless the different eigenfrequencies tend to infinity. Different from Eq. (9), the phase near the transmission dip does not change by π here. It is due to the nonvanishing value of coupling parameter q in the Fano spectrum [20], which qualitatively measures the interference between the bound states and the propagating continuum states.

VI. CONCLUSION

In conclusion, we have studied the effect of which-way detection inherent to a class of experimentally accessible systems with some intrinsic Mach-Zehnder interferometer

configuration to enjoy the quantum-classical interference of two virtual paths. This observation is used to explain the discovered progressive de-interference in the transmission spectrum of single photons propagating in a 1D CRA as the nonlocal couplings of a TLS to two nearest resonators increase its strength gradually. Besides the quantum realizations with the nano-electromechanical-resonator arrays where two nearest resonators with magnetic tips simultaneously interact with a single spin, the classical analog is proposed based on a waveguide of a coupled-defected cavity array with double couplings to a side-defected cavity.

We note that it seems there are two paths for the single photon (or boson) as shown in Fig. 1(a): direct coupling via coupling ξ (denoted as path 1) and indirect coupling via the TLS with coupling strengths $g0$ and $g1$ (denoted as path 2), which may make the whole interpretation simple. However, we would like to emphasize that path 1 is not a well-defined path for which-way detection for the following two reasons: First, let us review the double-slit experiment where a single photon passing through two independent paths (actually there might be infinite paths, but we can divide them into two parts by considering which slit the photon passes through) can exhibit an interference pattern far away from the two slits. It is said there are two paths because one can place a detector on any one of the two paths to directly identify which path the photon has taken. However, our setup is in the discrete coordinate space, and there are no media between resonator 0 and resonator 1 on path 1. Namely, one cannot use a detector to directly observe that the single photon indeed passes through path 1. Second, in the double-slit experiment, the amplitude of a photon at a fixed point far away from the slits is the sum of the two different paths. But in our model, the transmission amplitude is not a sum of those from paths 1 and 2. However, in the interpretation with paths B and D, one can identify which path the photon has taken by placing a detector on B or D, and the total transmission amplitude is exactly the sum of t_k^B and t_k^D, where t_k^B (t_k^D) are acquired by ignoring paths D (B). So paths B and D are well-defined independent paths. The introduction of operators B and D is necessary besides understanding the competition between the δ effective potentials and the effective dispersive coupling strength as well as the total transmission on the upper bound of the spectrum $g_0 = g_1$.

ACKNOWLEDGMENTS

This work was supported by the NSFC through Grants No. 10974209, No. 10935010, No. 11074071, and No. 11075050, the National 973 program (Grant No. 2012CB922103). Grant No. NCET-08-0682, PCSIRT Grant No. IRT0964, the Key Project of the Chinese Ministry of Education (Grant No. 210150), the Hunan Provincial Natural Science Foundation under Grant No. 11JJ7001, and the Scientific Research Fund of the Hunan Provincial Education Department (Grant No. 11B076).

[1] N. Bohr, Discussions with Einstein on Epistemological Problems in Atomic Physics, in *Albert Einstein: Philosopher Scientist*, edited by P. A. Schilpp (Library of Living Philosophers, Evanston, IL: Open Court Publishing, 1949), p. 218.

[2] W. H. Zurekk, Rev. Mod. Phys. **75**, 715 (2003).

[3] A. Stern, Y. Aharonov, and Y. Imry, Phys. Rev. A **41**, 3436 (1990).

[4] Y. Aharonov, D. Z. Albert, and L. Vaidman, Phys. Rev. Lett. **60**, 1351 (1988).

[5] E. Buks *et al.*, Nature (London) **391**, 871 (1998).

[6] S. Durt, T. Nonn, and G. Rampe, Nature (London) **395**, 33 (1998).

[7] R. Schuster *et al.*, Nature (London) **385**, 417 (1997).

[8] X. Y. Zou, L. J. Wang, and L. Mandel, Phys. Rev. Lett. **67**, 318 (1991).

[9] L. Zhou, Z. R. Gong, Y.-X. Liu, C. P. Sun, and F. Nori, Phys. Rev. Lett. **101**, 100501 (2008).

[10] L. Zhou, S. Yang, Y.-X. Liu, C. P. Sun, and F. Nori, Phys. Rev. A **80**, 062109 (2009).

[11] L. Zhou, H. Dong, Y.-X. Liu, C. P. Sun, and F. Nori, Phys. Rev. A **78**, 063827 (2008); Z. R. Gong, H. Ian, L. Zhou, and C. P. Sun, *ibid.* **78**, 053806 (2008).

[12] J. T. Shen and S. Fan, Phys. Rev. Lett. **95**, 213001 (2005).

[13] L. Zhou, F. M. Hu, J. Lu, and C. P. Sun, Phys. Rev. A **74**, 032102 (2006); L. Zhou, Y. B. Gao, Z. Song, and C. P. Sun, *ibid.* **77**, 013831 (2008).

[14] O. Astafiev, A. M. Zagoskin, A. A. Abdumalikov Jr. *et al.*, Science **327**, 840 (2010).

[15] J. D. Joannopoulos *et al.*, *Photonic Crystals Molding the Flow of Light* (Princeton University Press, Princeton, 2008).

[16] P. Rabl, S. J. Kolkowitz, F. H. L. Koppens *et al.*, Nat. Phys. **6**, 602 (2010).

[17] Y. Chang and C. P. Sun, Phys. Rev. A **83**, 053834 (2011).

[18] D. Z. Xu, H. Ian, T. Shi, H. Dong, and C. P. Sun, Sci. China Phys., Mech. Astron. **53**, 1234 (2010)

[19] J.-Q. Liao, Z. R. Gong, L. Zhou, Y.-X. Liu, C. P. Sun, and F. Nori, Phys. Rev. A **81**, 042304 (2010).

[20] U. Fano, Phys. Rev. **124**, 1866 (1961).